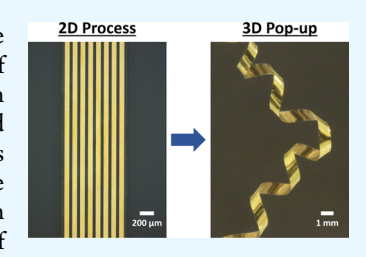


Responsive, 3D Electronics Enabled by Liquid Crystal Elastomer Substrates

Hyun Kim,^{†,§} John Gibson,^{‡,§} Jimin Maeng,^{†,§} Mohand O. Saed,[†] Krystine Pimentel,[‡] Rashed T. Rihani,[†] Joseph J. Pancrazio,[†] Stavros V. Georgakopoulos,[‡] and Taylor H. Ware^{*,†}

Supporting Information

ABSTRACT: Traditional electronic devices are rigid, planar, and mechanically static. The combination of traditional electronic materials and responsive polymer substrates is of significant interest to provide opportunities to replace conventional electronic devices with stretchable, 3D, and responsive electronics. Liquid crystal elastomers (LCEs) are well suited to function as such dynamic substrates because of their large strain, reversible stimulus response that can be controlled through directed self-assembly of molecular order. Here, we discuss using LCEs as substrates for electronic devices that are flat during processing but then morph into controlled 3D structures. We design and demonstrate processes for a variety of electronic devices on LCEs including deformation-tolerant conducting traces and capacitors



and cold temperature-responsive antennas. For example, patterning twisted nematic orientation within the substrate can be used to create helical electronic devices that stretch up to 100% with less than 2% change in resistance or capacitance. Moreover, we discuss self-morphing LCE antennas which can dynamically change the operating frequency from 2.7 GHz (room temperature) to 3.3 GHz (-65 °C). We envision applications for these 3D, responsive devices in wearable or implantable electronics and in cold-chain monitoring radio frequency identification sensors.

KEYWORDS: liquid crystal elastomers, flexible electronics, 3D electronics, capacitors, antennas

INTRODUCTION

Shape is a critical property of microelectronic devices that are designed to function in diverse applications such as sensors, 1,2 actuators, 3,4 human-machine interfaces, 5,6 soft robots, 7,8 and antennas.^{9,10} In these devices, the three-dimensional (3D) structure imparts functionality beyond what is achievable with two-dimensional (2D) structures. 11 For example, brittle materials fabricated into 2D structures, as is typically the case for microelectronics, may be flexible, but these devices are not stretchable. 3D architecture can impart extrinsic stretchability on devices that would be damaged by large deformations. In nature, for example, the ulnar nerve in humans and the ventral groove blubber nerve in whales are able to withstand large mechanical deformation without injury due to an intrinsic 3D architecture. 12 Furthermore, if 3D shape can be reconfigured during use, then the properties of the electronic device can be actively controlled. ¹³ For example, the radiation properties of antennas are directly tied to the shape of the conductor. Therefore, if the shape of an antenna can be controlled, the performance of wireless communication devices can be designed to be dynamic.

Traditional processing methods of thin-film electronics, such as photolithography, require 2D substrates and also require the use of heat, light, and solvents. As such, integration of electronic components into 3D, shape-changing structures is challenging. 14-16 Material strategies are needed to create electronic devices that are compatible with thin-film processing

methods and result in electronic devices where 3D shape can be dynamically and precisely controlled. Thus, to enable electronics in 3D structures, a variety of techniques have been described to morph 2D electronic structures into 3D including using residual stress-induced bucking or wrinkling 17-19 and patterning of rigid metal components into wavy or fractal patterns.²⁰ While many of these efforts have focused on controlling the 3D architecture of the rigid electronic components, reconfigurable substrates that morph from flat (during processing) to 3D (after processing) have also been designed. The advantage of this substrate reconfiguration approach is that the widely used processing techniques for thin-film materials (e.g., lithography) can be used. This shape transformation can be accomplished with shape-memory polymers, 21,22 stress-engineered substrates, 14 origami and kirigami techniques, ^{23,24} hydrogels, ²⁵ and buckling from elastic recovery. 26,27

Liquid crystal elastomers (LCEs)²⁸⁻³⁰ are a class of shapechanging materials where directed self-assembly can be used to define the reversible shape change of the substrate in a voxelby-voxel manner on the micrometer scale.³¹ Notably, these materials are also well suited to function as dielectrics as compared to hydrogels or other smart materials that are ionic

Received: March 7, 2019 Accepted: May 9, 2019 Published: May 9, 2019



[†]Department of Bioengineering, The University of Texas at Dallas, Richardson, Texas 75080, United States

^{*}Department of Electrical and Computer Engineering, Florida International University, Miami, Florida 33174, United States

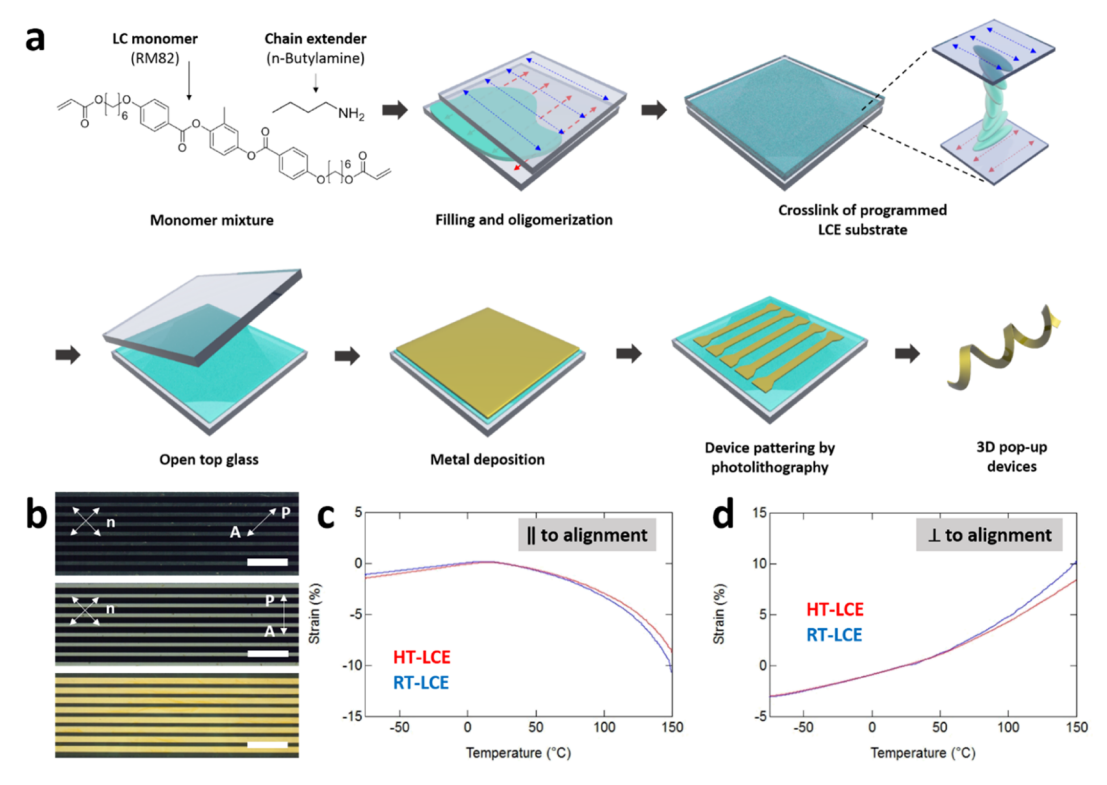


Figure 1. Overview of LCE chemistry, device fabrication, and thermomechanical properties. (a) Schematic drawing of molecular structures and fabrication process. (b) Polarized optical micrographs and reflection micrograph of gold traces on an LCE. Isoforce measurements of uniaxially aligned LCEs along (c) and perpendicular (d) to the alignment. (Scale bar = $500 \ \mu m$).

conductors.³² While shape change in LCEs is often triggered by heating through an order-disorder transition,³³ shape for these materials should be considered as a property that varies more widely with temperature (i.e., on both heating and cooling), as shape change is also observed because of anisotropic coefficients of thermal expansion (CTE). To realize shape-morphing, 3D electronics, we use LCEs as dynamic substrates for electronics that are processable using photolithography and then reconfigurable from 2D to 3D postfabrication. To control this reconfiguration, we design the stimulus response of the LCEs using photoalignment. In this research, we achieve 3D transformation not by heating but instead by cooling below the cross-linking temperature. Using this approach, we demonstrate the first examples of 3Darchitectured microscale electronic devices enabled by the shape change of LCEs. The devices demonstrated include strain-tolerant conducting traces and metal-insulator-metal (MIM) capacitors that are designed to operate at temperatures near room temperature. We also demonstrate antennas that dynamically change their radiation properties in response to changing temperature well below 0 °C.

■ RESULTS AND DISCUSSION

LCE substrates were formed with a one-pot, two-step reaction resulting in photolithography-compatible, planar substrates with programmed stimulus response. Briefly, the LCE precursors are filled into a glass cell. The cell consists of a pair of glass slides each coated with an azobenzene-based dye separated by a gap of 37 μ m. Photoalignment of the azobenzene dye can be induced by exposure to linearly polarized light, which ultimately controls the orientation of the LCE precursors and can be used to design the stimulus response of the substrate. After filling, the monomer mixture

undergoes step-growth oligomerization resulting in acrylatecapped, main-chain, liquid crystal macromers. The macromers are subsequently cross-linked by photopolymerization. After cross-linking, the prepared LCE substrate remains on one of the glass slides for the lithography processes. Then, we deposit and pattern thin-film metals or dielectrics to build microelectronics, as shown in Figure 1a. Example structures of patterned microscale conducting traces on an oriented (twisted nematic) LCE substrate are shown in the polarized optical micrographs (POM) and reflection micrograph in Figure 1b. A characteristic dark and bright optical pattern is observed when rotating the samples between parallel polarizers; this confirms that micropatterned electronics were successfully fabricated on twisted nematic 2D LCE substrates. It should be emphasized that thermal and chemical processing conditions of the photolithography process were compatible with our LCE adhered to a carrier substrate, even though LCEs undergo large changes in shape on heating as freestanding materials.

After this 2D photolithography process, LCE-based devices can morph from flat to 3D shapes when released from the carrier substrate. It should be noted that additional thermal or mechanical processing, which could damage thin-film electronics, is not required to obtain the designed 3D structure. Instead, this programmed pop-up shape transition is based on the molecular orientation of the LCEs set during synthesis by cross-linking of LCEs at an elevated temperature. The cross-linking temperature sets the temperature at which the film later is in the planar state. To be more specific, in the 3D substrate preparation process, we align the monomer mixture and then oligomerize this mixture. Before we cross-link, we elevated the temperature to 90 °C. At this temperature, the twisted nematic oligomer retains order. We cross-link the mixture in this condition, thus setting the temperature at which

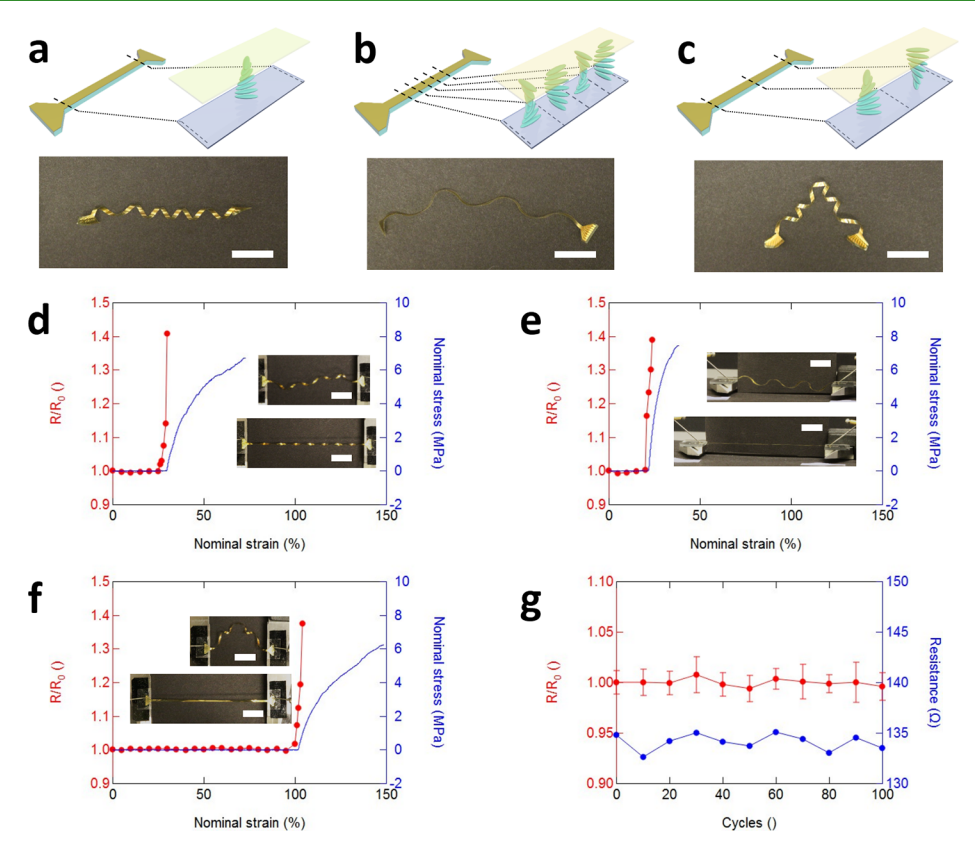


Figure 2. 3D pop-up LCE with conducting traces. Schematic illustrations and optical images of 3D LCE with conducting traces in helix (a), wavy (b), and helical inversion (c) geometries. Representative resistance-strain and stress-strain curves of LCE conducting traces in helix (d), wavy (e), and helical inversion (f) geometries. Nominal stress is defined by dividing load by the cross-sectional area of the flat device. (g) Reversible straintolerant performance of the helical inversion device for 100 cycles of strain and release ($\varepsilon = 0-90\%$). (Scale bar = 1 cm).

the film is flat to be near 90 °C. Thus, on subsequent release from the glass substrate, anisotropic shrinking occurs (~4% strain along the alignment and ~3.5% strain perpendicular to the alignment), as dictated by the magnitude of the temperature difference between room temperature and the cross-linking temperature. When the molecular order is patterned with an off-axis twist through the structure, the LCE forms out-of-plane twisted 3D structures at room temperature (Figure S1). By maximizing the change in the temperature between the cross-linking temperature and the use temperature, the strain at the use temperature can be maximized. We note that the nematic-to-isotropic transition temperature $(T_{ni} = \sim 100 \, ^{\circ}\text{C} \text{ of the oligomer})^{31}$ cannot be exceeded prior to cross-linking, or the programmed orientation would be lost. As we cross-link in the nematic phase, the substrates show characteristic birefringence as shown in Figure

To quantify the shape change resulting from cooling below the polymerization temperature, we measure dimensional changes as a function of temperature and molecular orientation. We note that the reversible shape changes of this LCE system in response to high temperature have been previously reported, 31 but in this work, we effectively use the response on cooling the material below the cross-linking temperature. As evident in Figure 1c,d, shape change in uniaxially aligned samples between -75 and 150 °C is observed in the absence of a load. Both the heating and cooling temperature response is caused by anisotropy in CTE of the nematic LCEs. Room-temperature cross-linked LCEs (RT-LCEs) exhibit $11.3 \pm 1.2\%$ (n = 3, mean \pm stdev) contraction

along the director and $10.6 \pm 0.7\%$ expansion perpendicular to the director at 150 °C. High-temperature (90 °C) cross-linked LCEs (HT-LCEs) show slightly smaller deformation with 9.6 \pm 0.5% contraction along the director and 8.9 \pm 1.1% expansion perpendicular to the director at 150 °C. Importantly, the actuation of LCEs is not only limited to high temperature but also occurs at temperatures below room temperature. When RT-LCEs are cooled from room temperature to -75 °C, anisotropic contractions of around 0.6 ± 0.6 and $3.2 \pm 0.2\%$ are measured along and perpendicular to the alignment direction, respectively. Similarly, HT-LCEs contract around 0.9 \pm 0.5 and 2.7 \pm 0.3% along and perpendicular to the alignment, respectively. Here, we employ this thermomechanical anisotropy to create electronics that deploy from flat to 3D and to create dynamic electronics that sense and respond to temperature changes.

By creating elastomeric substrates that morph into 3D geometries, we seek to imbue extrinsic stretchability to electronic devices. Stretchable electronic devices should function through a wide range of out-of-plane deformations including bending or twisting.36,37 It is well known that metallic thin-film electronic materials are brittle with failure strains on the order of 1%. 26,27 To create extrinsically stretchable substrates, we program the molecular orientation of LCE substrates with variation both through the thickness and within the plane of the substrate, as shown in the illustrations from Figure 2a-c. Devices, in this case simple microscale conducting traces, reconfigure from 2D to helical (Figure 2a), wavy (Figure 2b), and helical with a handedness inversion (Figure 2c) geometries after fabrication. Notably,

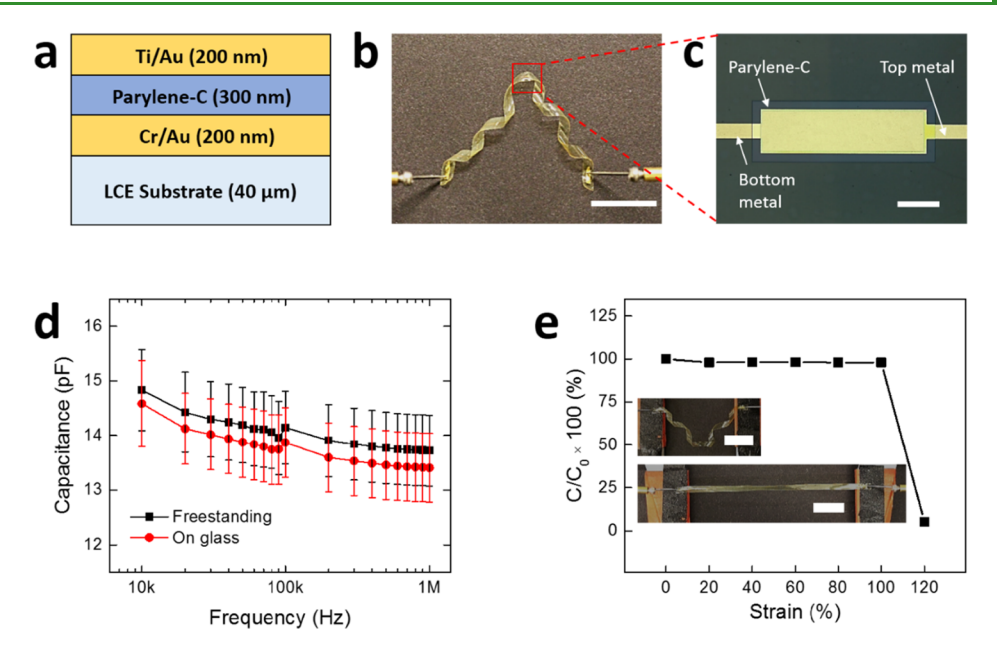


Figure 3. 3D pop-up LCE-MIM-Cap. (a) Schematic cross section of the LCE-MIM-Cap structure. (b) Optical image of LCE-MIM-Cap in helical inversion geometry. (Scale bar = 1 cm) (c) Reflection micrograph of the LCE-MIM-Cap. (Scale bar = $200 \, \mu \text{m}$) (d) Capacitance in the frequency range of 10 kHz to 1 MHz on the flat 2D geometry and 3D pop-up geometry. (e) Representative strain tolerant capacitance (at 1 MHz) under stretching deformation. (Scale bar = 1 cm).

this shape is controlled by both the alignment of the substrate and the cross-linking temperature (90 °C). The characteristic birefringence of these patterned structures is shown in Figure S3a,b. The resulting 3D devices consist of patterned thin-film gold traces that are electrically conductive on the programmed LCE substrates. These elastic 3D structures of LCEs are extrinsically stretchable much like a telephone cord, thus protecting the intrinsically brittle electronics from deformation. On stretching, helical devices undergo macroscopic deformation from loosely coiled to tightly coiled as shown in Figures 2d and S4a. It should be noted that electrical failure (~31%) was observed very near the inflection point in the stress-strain curve associated with stretching of the substrate (~30%). Wavy devices undergo deformation from wavy to flat as shown in Figures 2e and S4b. Similarly, the electrical failure strain (\sim 24%) was observed near the inflection point (\sim 23%) in the stress-strain curve. Lastly, helical devices with a handedness inversion, which results in both bend and twist, show larger electrical failure strain (~104%) just above the inflection point in the stress-strain curve (\sim 102%) as shown in Figures 2f and S4c. At strains below the failure strain, these devices can be reversibly deformed without electrical failure. For the helical inversion device, the device survived 100 cycles of 90% strain and release as shown in Figure 2g. These results clearly show that the mechanical failure mechanism of thin-film electronics may be controlled with the shape of the electronic device. Transmission optical micrographs were taken below and above the electrical failure strain of the devices. Cracks are absent from the devices until the failure strain is reached (Figure S4d-f). We note that LCE-based helical devices have smaller bending stiffness than twisting stiffness as devices undergo unwinding when pulled.³⁸ Unwinding and rewinding of the device during deformation is shown in Movie S1. Overall, in each of these 3D geometries, electrical failure occurs immediately after (~1% strain) the inflection point in the stress-strain curve that is associated with a transition from bending-dominated deformation to stretching.

It should be noted that failure mechanisms are different between helical devices and wavy or helical inversion devices. Because wavy and helical inversion devices have net zero twist, the devices stretch from 3D to flat. However, the helical device with only a single handedness reconfigures from a helix to a helicoid by stretching. We note, each conducting trace was fabricated to have the same 5.5 cm metal length. However, based on the patterned molecular orientation in LCE substrates, devices can pop-up into programmed 3D geometries which have different natural lengths, ~4.2 cm in helical, ~4.6 cm in wavy, and ~2.7 cm in helical inversion devices, respectively. In accordance with experimental results of helical inversion and wavy devices, electrical failure strain can be predicted by $(L_{\rm 2D}-L_{\rm 3D})/L_{\rm 2D}\times 100$. The length in 2D is denoted by $L_{\rm 2D}$, and the length of the initial 3D pop-up natural state is denoted by $L_{\rm 3D}$. It should be noted that failure strain of one handedness helical devices should be smaller than this calculation, as these devices are unable to untwist during stretching (Figure S4). In addition to being stretchable, 3D devices can be designed to resist torsion at isometric length as shown in Figure S5. The helical inversion device maintains its original performance (<2% resistance change) in the range of ± 10 turns (3600° twisting) (Figure S5a,c red). In the case of one handedness helical devices (Figure S5b,c blue), resistance was maintained when twisted seven turns; this resistance then slightly increased (6.1%) until 10 turns of twisting when twisted in the same handedness as the existing helix. However, when the helical device undergoes twist deformation of opposite handedness as the helix, knots were formed which cause length reduction, stress concentration, and electrical failure. Also, in the case of flat devices, electrical failure was observed within 2 turns of isometric length twisting deformation (Figure S5c black).

So far, we have demonstrated the feasibility of single-layered microscale conducting traces fabrication on programmed LCE substrates. The processes we describe here are also suitable for building multilayer electronic devices. MIM capacitors are one

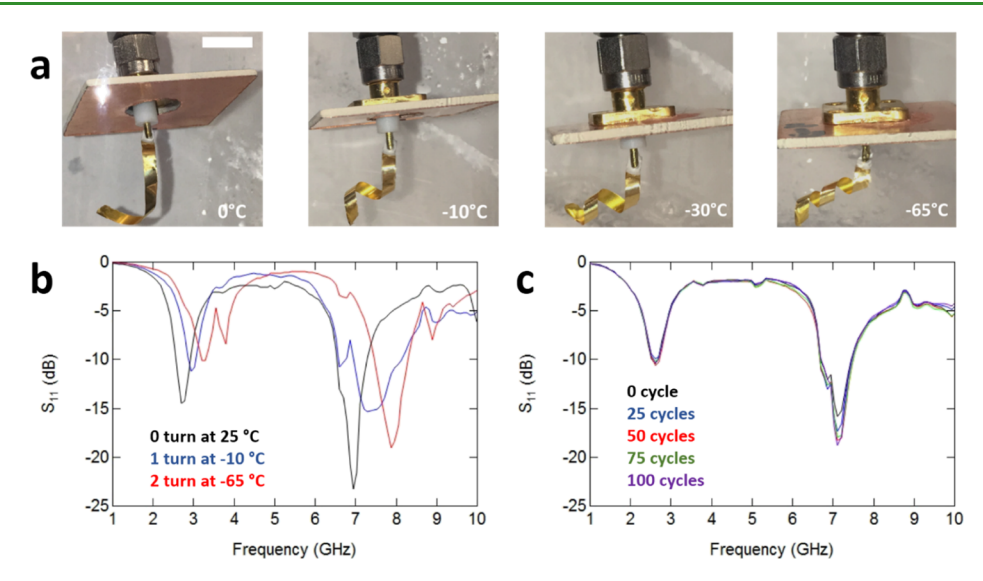


Figure 4. Cold-temperature sensing LCE antenna. (a) Shape-shifting of LCE antenna as function of temperature. (b) Measured reflection coefficient (S_{11}) of the LCE antenna as the number of turns increased as temperature decreases. (c) Measured frequency response of the reflection coefficient (S_{11}) after the LCE antenna has been reversibly actuated through cold temperatures from 0 to 100 cycles. (Scale bar = 1 cm).

of the key building blocks in integrated circuit technology.^{39,40} Owing to their merits of low mass and volume, high electrical performance, and high reliability, MIM capacitors can allow significant miniaturization of electronic systems by complementing or even replacing surface-mount discrete capacitors.⁴¹ However, integration of MIM capacitors into stretchable electronics is difficult because rigid metal and dielectric elements are limited by strain-induced damage. 42 Here, we demonstrate fabrication of MIM capacitors onto LCEs (LCE-MIM-Cap). Figure 3a illustrates the configuration of the MIM capacitors implemented in this work. On top of an oriented LCE film, a thin-film metal (Cr/Au, 200 nm)-insulator (parylene-C, 300 nm)-metal (Ti/Au, 200 nm) multilayer is deposited and patterned. Figure 3b shows an example of a fabricated MIM capacitor on a freestanding LCE film with the active device area magnified in Figure 3c. Here, the deformation of the LCE film into a helix with a handedness inversion occurs naturally upon releasing the LCE film from the carrier glass, as we cross-linked this substrate at 90 °C. For electrical characterization, we first measure and compare the capacitance of the fabricated LCE-MIM-Cap before and after releasing the devices from the glass substrate (labeled as "On glass" and "Freestanding", respectively) as shown in Figure 3d. The as-fabricated, flat capacitors exhibit capacitances of 14.6-13.4 pF in the frequency range of 10 kHz to 1 MHz. These values correspond to capacitance densities of 9.1-8.4 nF/cm², which is reasonable for a 300 nm-thick parylene-C dielectric.⁴³ The dielectric constant of parylene-C is calculated as 3.09, 2.94, and 2.84 at 10 kHz, 100 kHz, and 1 MHz, respectively. These values agree closely with those reported in the literature. 44 After being released and deformed, the LCE-MIM-Cap still maintain capacitances of 14.8-13.7 pF, which is close to their original values with only a small deviation of 1.5-2.3% in the entire frequency range. These capacitors exhibit high tolerance against voltage biases from -5 to +5 V, where a stable capacitance value of ~13.255 pF is maintained as shown in Figure S6a. The released helical inversion LCE-MIM-Cap also exhibits high strain tolerance under stretching conditions as shown in Figures 3e and S7. Under gradual increment of strain from 0 to 100% ($\Delta = 20\%$), the capacitors retained

~98% of their original capacitance. The devices failed under a 120% strain, where the LCE strip was fully stretched. The occurrence of the failure at full stretch agrees well with the case shown for the resistance changes in Figure 2f. It is worth noting that scalable capacitances ranging from 1.7 to 55 pF have been achieved for various capacitor areas from 2×10^{-4} to 6.4×10^{-3} cm² as shown in Figure S6b. This range of capacitance values is well suited for radio frequency applications in filtering, timing, and termination. The stable operation of the MIM capacitors after release from the substrate and during stretching offers promise for the use of this technology in stretchable smart electronics. In addition, the successful fabrication of multilayer thin-film capacitors on an LCE platform opens up new possibilities for implementing active electronic devices, possessing similar multilayer configurations, on LCE; possible candidates include lowtemperature processed thin-film transistors and diodes. 45,46

So far, we have focused on electronics that are stretchable near room temperature. However, the reversible shapechanging properties of LCEs can also be used to create electronics that dynamically reshape. We previously reported a high-temperature-responsive antenna based on LCE coated with an aluminum foil.⁴⁷ Here, LCEs are developed that can be programmed to provide specific and reversible changes in their shape as temperature changes from room temperature to cold temperatures. These LCEs are used as substrates for novel antennas to enable new battery-less, nonvisual, and reusable temperature sensors that are capable of real-time temperature monitoring and detection. Smart packaging has the potential to significantly improve the traceability, safety, and quality of temperature-sensitive goods, such as food and medicines.⁴⁸ Currently, limited control of the supply chain leads to nearly 20% loss of fresh food postharvest, resulting in significant financial loss and environmental burden. 49 As a result of this loss, smart packaging has emerged as a leading strategy to provide local monitoring of the condition of the shipped goods. For example, a variety of temperature-indicating labels have been developed to indicate when a maximum temperature has been exceeded. Typically, these devices are color-changing indicators. These sensors require a direct line of sight to the

Table 1. Measured Resonant Frequency and Bandwidth of Dual-Band LCE Antenna Versus Temperature

LCE antenna		band 1			band 2		
# of turns	temperature (°C)	frequency (GHz)	S_{11} (dB)	BW10dB (MHz)	frequency (GHz)	S ₁₁ (dB)	BW10dB (MHz)
0	25	2.7	-14.5	370	6.95	-23.3	750
1	-10	2.96	-11.2	180	7.29	-15.4	1190
2	-65	3.3	-10.1	10	7.89	-19.1	850

sensor and are inefficient to read in bulk. Furthermore, once "triggered", these sensors no longer provide useful data and must be discarded.⁵⁰ Thus, here we develop reversibly selfmorphing monopole LCE antennas that morph into helical antennas and dynamically change operating frequency in response to cold temperatures. To realize cold temperaturesensitive LCE antenna, we prepared twisted nematic, roomtemperature cross-linked LCE substrates which are flat at room temperature and helical at cold temperatures (Figure S8a). The prepared LCEs were then coated with 200 nm gold. The gold-coated LCEs were cut along 45° to the director as illustrated in Figure S8b. The resulting LCE antennas are flat at room temperature (Figure S8c). The LCE antenna was evaluated at temperatures below 0 °C. Figure 4a shows the LCE antenna changing shape as a function of temperature. As the LCE antenna is lowered into a flask with a mixture of dry ice and isopropanol (-78 °C), the temperature decreases, which changes the shape of the antenna from flat to a helical shape. It is important to note that as the temperature decreases, the number of turns of the helix formed by the LCE increases. The mechanical deformation into 3D helix geometry of LCE antennas is caused by thermomechanical anisotropy of the LCE substrates as described in Figure 1c,d. In other words, when the molecular order is patterned with an off-axis twist through the structure, anisotropic CTE of the LCE substrate induces out-of-plane twisting deformation by either heating or cooling. In this case, only the anisotropic CTE of the LCE is required for twisting. The difference in CTE between the LCE and the metal were not found to contribute significantly to the shape change (Figure S9). Figure 4b shows the reflection coefficient, S_{11} , of the LCE antenna for three different temperatures. Specifically, the LCE antenna morphs from having zero to one, and then to two turns (corresponding to 25, -30, and -65 °C, respectively). Figure 4b also illustrates that in the frequency range between 1 and 10 GHz, the LCE antenna has two operating frequency bands, which are summarized in Table 1. The bandwidth is defined as the frequencies where $S_{11} \leq -10$ dB and S_{11} are shown at the center frequency. It should be noted that at room temperature, the LCE antenna has zero turns and performs as a monopole antenna. The operating frequency of the antenna increases as the temperature decreases (i.e., as the number of helical turns increases). This frequency shift occurs because as the LCE antenna twist increases, the current distribution and location of these currents in space change, which in turn changes its input impedance, reflection coefficient, and operating frequency. This frequency shift can be used to detect temperature change by using a transmitter that sends an interrogating signal to the LCE antenna to determine its operating frequency. Thus, changes in shape can indicate changes in temperature. Specifically, when the interrogating transmitter determines that the frequency of operation of the LCE antenna is 2.7, 2.96, or 3.3 GHz, then the sensed temperature will be 25, -10, or -65 °C, respectively. Figure 4c shows the measured reflection coefficient at room temperature after the LCE antenna has

been actuated repeatedly (each cycle takes the antenna from room temperature to -65 °C and back to room temperature). The LCE antenna after 100 cycles exhibits approximately the same resonant frequency in both bands of operation, which demonstrates robustness of this design. Notably, the mechanics of the morphing substrate can be affected by thin-film electronics. For future devices comprised of stiffer electronics, strategies to increase substrate thickness via layering⁵¹ or elastic modulus via crystallization⁵² or vitrification may be required.

CONCLUSIONS

We report routes to fabricate previously inaccessible classes of 3D, responsive electronics, including strain and deformationtolerant conducting traces, MIM capacitors, and frequency shifting antennas. Strain tolerance and antenna performance are controlled by using the programmable molecular orientation in LCEs, which controls the shape of these materials at a given temperature. Designing molecular orientation in LCE substrates enables further programmed 3D geometry with the controlled aspect ratio or spring index in the wavy or helical structure, respectively, thus achieving tunable performances in devices.

ASSOCIATED CONTENT

Supporting Information

The Supporting Information is available free of charge on the ACS Publications website at DOI: 10.1021/acsami.9b04189.

Experimental details of LCE substrate and device preparation; LCE shape as controlled by polymerization temperature, polarized optical micrographs of LCEs with patterned director orientation, macroscopic deformation of LCE devices, capacitance as a function of voltage bias, capacitance as a function of strain, antenna fabrication, effect of metal on 3D shape; and antenna analysis (PDF)

Unwinding and rewinding of the helical inversion device during deformation (MP4)

AUTHOR INFORMATION

Corresponding Author

*E-mail: taylor.ware@utdallas.edu.

ORCID ®

Taylor H. Ware: 0000-0001-7996-7393

Author Contributions

§H.K., J.G., and J.M. contributed equally.

The authors declare no competing financial interest.

ACKNOWLEDGMENTS

This research was partially supported by the National Science Foundation under grant no. 1711383 and partially supported by the Defense Advanced Research Projects Agency (DARPA) under contract no. 140D6318C0097. The authors from Florida International University would like to acknowledge the support by the following grants: NSF ECCS 1711467 and NSF EFRI 1332348 (co-funded by AFOSR). J.G. and K.P. would like to thank the Florida Education Fund McKnight Doctoral Fellowship, Florida International University (FIU) Graduate School Enhancement, and the National Science Foundation Florida Georgia LSAMP FIU Bridge to the Doctorate HRD #1301998 for the financial support. Special thanks to Prof. Habeom Lee for his generous help and time in 3D schematic illustrations.

REFERENCES

- (1) Gerratt, A. P.; Michaud, H. O.; Lacour, S. P. Elastomeric Electronic Skin for Prosthetic Tactile Sensation. Adv. Funct. Mater. 2015, 25, 2287-2295.
- (2) Mishra, S.; Norton, J. J. S.; Lee, Y.; Lee, D. S.; Agee, N.; Chen, Y.; Chun, Y.; Yeo, W.-H. Soft, Conformal Bioelectronics for a Wireless Human-Wheelchair Interface. Biosens. Bioelectron. 2017, 91, 796-803
- (3) Schaffner, M.; Faber, J. A.; Pianegonda, L.; Rühs, P. A.; Coulter, F.; Studart, A. R. 3D Printing of Robotic Soft Actuators with Programmable Bioinspired Architectures. Nat. Commun. 2018, 9, 878.
- (4) de Haan, L. T.; Gimenez-pinto, V.; Konya, A.; Nguyen, T.; Verjans, J. M. N.; Sánchez-somolinos, C.; Selinger, J. V.; Selinger, R. L. B.; Broer, D. J.; Schenning, A. P. H. J. Accordion-like Actuators of Multiple 3D Patterned Liquid Crystal Polymer Films. Adv. Funct. Mater. 2014, 24, 1251-1258.
- (5) Herbert, R.; Kim, J. H.; Kim, Y. S.; Lee, H. M.; Yeo, W. H. Soft Material-Enabled, Flexible Hybrid Electronics for Medicine, Healthcare, and Human-Machine Interfaces. Materials 2018, 11, 187.
- (6) Jeong, J.-W.; Yeo, W.-H.; Akhtar, A.; Norton, J. J. S.; Kwack, Y.-J.; Li, S.; Jung, S.-Y.; Su, Y.; Lee, W.; Xia, J.; et al. Materials and Optimized Designs for Human-Machine Interfaces via Epidermal Electronics. Adv. Mater. 2013, 25, 6839-6846.
- (7) Kim, S.; Laschi, C.; Trimmer, B. Soft Robotics: A Bioinspired Evolution in Robotics. Trends Biotechnol. 2013, 31, 287-294.
- (8) Wang, C.; Sim, K.; Chen, J.; Kim, H.; Rao, Z.; Li, Y.; Chen, W.; Song, J.; Verduzco, R.; Yu, C. Soft Ultrathin Electronics Innervated Adaptive Fully Soft Robots. Adv. Mater. 2018, 30, 1706695.
- (9) Costantine, J.; Tawk, Y.; Barbin, S. E.; Christodoulou, C. G. Reconfigurable Antennas: Design and Applications. Proc. IEEE 2015, 103, 424-437.
- (10) Hayes, G. J.; Liu, Y.; Genzer, J.; Lazzi, G.; Dickey, M. D. Self-Folding Origami Microstrip Antennas. IEEE Trans. Antennas Propag. 2014, 62, 5416-5419.
- (11) Rogers, J. A.; Someya, T.; Huang, Y. Materials and Mechanics for Stretchable Electronics. Science 2010, 327, 1603-1607.
- (12) Shah, S. B. Tissue Biomechanics: Whales Have Some Nerve. Curr. Biol. 2017, 27, R177-R179.
- (13) Zhu, J.; Dexheimer, M.; Cheng, H. Reconfigurable Systems for Multifunctional Electronics. npj Flex. Electron. 2017, 1, 8.
- (14) Sundaram, S.; Kim, D. S.; Baldo, M. A.; Hayward, R. C.; Matusik, W. 3D-Printed Self-Folding Electronics. ACS Appl. Mater. Interfaces 2017, 9, 32290-32298.
- (15) Wang, H.; Wang, Y.; Tee, B. C. K.; Kim, K.; Lopez, J.; Cai, W.; Bao, Z. Shape-Controlled, Self-Wrapped Carbon Nanotube 3D Electronics. Adv. Sci. 2015, 2, 1500103.
- (16) Frick, C. P.; Merkel, D. R.; Laursen, C. M.; Brinckmann, S. A.; Yakacki, C. M. Copper-Coated Liquid-Crystalline Elastomer via Bioinspired Polydopamine Adhesion and Electroless Deposition. Macromol. Rapid Commun. 2016, 37, 1912-1917.
- (17) De Haan, L. T.; Leclère, P.; Damman, P.; Schenning, A. P. H. J.; Debije, M. G. On-Demand Wrinkling Patterns in Thin Metal Films Generated from Self-Assembling Liquid Crystals. Adv. Funct. Mater. 2015, 25, 1360-1365.

- (18) Lee, D. W.; Lee, J. H.; Jin, J.-H. Innovative Evolution of Buckling Structures for Flexible Electronics. Compos. Struct. 2018, 204, 487-499.
- (19) Lacour, S. P.; Wagner, S.; Huang, Z.; Suo, Z. Stretchable Gold Conductors on Elastomeric Substrates. Appl. Phys. Lett. 2003, 82,
- (20) Fan, J. A.; Yeo, W.; Su, Y.; Hattori, Y.; Lee, W.; Jung, S.; Zhang, Y.; Liu, Z.; Cheng, H.; Falgout, L.; et al. Fractal Design Concepts for Stretchable Electronics. Nat. Commun. 2014, 5, 3266.
- (21) Liu, C.; Qin, H.; Mather, P. T. Review of Progress in Shape-Memory Polymers. J. Mater. Chem. 2007, 17, 1543-1558.
- (22) Reeder, J. T.; Kang, T.; Rains, S.; Voit, W. 3D, Reconfigurable, Multimodal Electronic Whiskers via Directed Air Assembly. Adv. Mater. 2018, 30, 1706733.
- (23) Shyu, T. C.; Damasceno, P. F.; Dodd, P. M.; Lamoureux, A.; Xu, L.; Shlian, M.; Shtein, M.; Glotzer, S. C.; Kotov, N. A. A Kirigami Approach to Engineering Elasticity in Nanocomposites through Patterned Defects. Nat. Mater. 2015, 14, 785-789.
- (24) Xu, L.; Shyu, T. C.; Kotov, N. A. Origami and Kirigami Nanocomposites. ACS Nano 2017, 11, 7587-7599.
- (25) Yu, C.; Duan, Z.; Yuan, P.; Li, Y.; Su, Y.; Zhang, X.; Pan, Y.; Dai, L. L.; Nuzzo, R. G.; Huang, Y.; et al. Electronically Programmable, Reversible Shape Change in Two- and Three-Dimensional Hydrogel Structures. Adv. Mater. 2013, 25, 1541-1546.
- (26) Xu, F.; Lu, W.; Zhu, Y. Controlled 3D Buckling of Silicon Nanowires for Stretchable Electronics. ACS Nano 2010, 5, 672-678.
- (27) Sun, Y.; Choi, W. M.; Jiang, H.; Huang, Y. Y.; Rogers, J. A. Controlled Buckling of Semiconductor Nanoribbons for Stretchable Electronics. Nat. Nanotechnol. 2006, 1, 201-207.
- (28) Küpfer, J.; Finkelmann, H. Nematic Liquid Single Crystal Elastomers. Makromol. Chem. Rapid Commun. 1991, 12, 717-726.
- (29) White, T. J.; Broer, D. J. Programmable and Adaptive Mechanics with Liquid Crystal Polymer Networks and Elastomers. Nat. Mater. 2015, 14, 1087-1098.
- (30) Ula, S. W.; Traugutt, N. A.; Volpe, R. H.; Patel, R. R.; Yu, K.; Yakacki, C. M. Liquid Crystal Elastomers: An Introduction and Review of Emerging Technologies. Liq. Cryst. Rev. 2018, 6, 78-107. (31) Ware, T. H.; McConney, M. E.; Wie, J. J.; Tondiglia, V. P.; White, T. J. Voxelated Liquid Crystal Elastomers. Science 2015, 347,
- (32) Rihani, R.; Kim, H.; Black, B.; Atmaramani, R.; Saed, M.; Pancrazio, J.; Ware, T. Liquid Crystal Elastomer-Based Microelectrode Array for In Vitro Neuronal Recordings. Micromachines 2018, 9, 416.
- (33) Wermter, H.; Finkelmann, H. Liquid Crystalline Elastomers as Artificial Muscles. E-Polymers 2001, 1, 1-13.
- (34) Sawa, Y.; Ye, F.; Urayama, K.; Takigawa, T.; Gimenez-Pinto, V.; Selinger, R. L. B.; Selinger, J. V. Shape Selection of Twist-Nematic-Elastomer Ribbons. Proc. Natl. Acad. Sci. U. S. A. 2011, 108, 6364-
- (35) Iamsaard, S.; Aßhoff, S. J.; Matt, B.; Kudernac, T.; Cornelissen, J. J. L. M.; Fletcher, S. P.; Katsonis, N. Conversion of Light into Macroscopic Helical Motion. Nat. Chem. 2014, 6, 229-235.
- (36) Ahn, J.-H.; Je, J. H. Stretchable Electronics: Materials, Architectures and Integrations. J. Phys. D: Appl. Phys. 2012, 45,
- (37) Ware, T. H.; Biggins, J. S.; Shick, A. F.; Warner, M.; White, T. J. Localized Soft Elasticity in Liquid Crystal Elastomers. Nat. Commun. **2016**, 7, 10781.
- (38) Gerbode, S. J.; Puzey, J. R.; McCormick, A. G.; Mahadevan, L. How the Cucumber Tendril Coils and Overwinds. Science 2012, 337, 1087-1091.
- (39) Ng, C. H.; Ho, C.-S.; Chu, S.-F. S.; Sun, S.-C. MIM Capacitor Integration for Mixed-Signal/RF Applications. IEEE Trans. Electron Devices 2005, 52, 1399-1409.
- (40) Jain, R.; Geuskens, B. M.; Kim, S. T.; Khellah, M. M.; Kulkarni, J.; Tschanz, J. W.; De, V. A 0.45-1 V Fully-Integrated Distributed Switched Capacitor DC-DC Converter with High Density MIM

- Capacitor in 22 Nm Tri-Gate CMOS. *IEEE J. Solid State Circuits* **2014**, 49, 917–927.
- (41) Roozeboom, F.; Kemmeren, A. L. A. M.; Verhoeven, J. F. C.; Van Den Heuvel, F. C.; Klootwijk, J.; Kretschman, H.; Frič, T.; Van Grunsven, E. C. E.; Bardy, S.; Bunel, C.; et al. Passive and Heterogeneous Integration towards a Si-Based System-in-Package Concept. *Thin Solid Films* **2006**, *504*, 391–396.
- (42) Sekitani, T.; Zschieschang, U.; Klauk, H.; Someya, T. Flexible Organic Transistors and Circuits with Extreme Bending Stability. *Nat. Mater.* **2010**, *9*, 1015–1022.
- (43) Maeng, J.; Kim, B.; Ha, D.; Chappell, W. J. Parylene Interposer as Thin Flexible 3-D Packaging Enabler for Wireless Applications. *IEEE Trans. Microwave Theory Tech.* **2011**, *59*, 3410–3418.
- (44) Kahouli, A.; Sylvestre, A.; Ortega, L.; Jomni, F.; Yangui, B.; Maillard, M.; Berge, B.; Robert, J.-C.; Legrand, J. Structural and Dielectric Study of Parylene C Thin Films. *Appl. Phys. Lett.* **2009**, *94*, 152901.
- (45) Nomura, K.; Ohta, H.; Takagi, A.; Kamiya, T.; Hirano, M.; Hosono, H. Room-Temperature Fabrication of Transparent Flexible Thin-Film Transistors Using Amorphous Oxide Semiconductors. *Nature* **2004**, 432, 488–492.
- (46) Zhang, J.; Wang, H.; Wilson, J.; Ma, X.; Jin, J.; Song, A. Room Temperature Processed Ultrahigh-Frequency Indium-Gallium-Zinc-Oxide Schottky Diode. *IEEE Electron Device Lett.* **2016**, *37*, 389–392.
- (47) Gibson, J. S.; Liu, X.; Georgakopoulos, S. V.; Wie, J. J.; Ware, T. H.; White, T. J. Reconfigurable Antennas Based on Self-Morphing Liquid Crystalline Elastomers. *IEEE Access* **2016**, *4*, 2340–2348.
- (48) Ghaani, M.; Cozzolino, C. A.; Castelli, G.; Farris, S. An Overview of the Intelligent Packaging Technologies in the Food Sector. *Trends Food Sci. Technol.* **2016**, *51*, 1–11.
- (49) Defraeye, T.; Cronjé, P.; Berry, T.; Opara, U. L.; East, A.; Hertog, M.; Verboven, P.; Nicolai, B. Towards Integrated Performance Evaluation of Future Packaging for Fresh Produce in the Cold Chain. *Trends Food Sci. Technol.* **2015**, *44*, 201–225.
- (50) Biji, K. B.; Ravishankar, C. N.; Mohan, C. O.; Srinivasa Gopal, T. K. Smart Packaging Systems for Food Applications: A Review. *J. Food Sci. Technol.* **2015**, *52*, 6125–6135.
- (51) Guin, T.; Settle, M. J.; Kowalski, B. A.; Auguste, A. D.; Beblo, R. V.; Reich, G. W.; White, T. J. Layered Liquid Crystal Elastomer Actuators. *Nat. Commun.* **2018**, *9*, 2531.
- (52) Kim, H.; Boothby, J. M.; Ramachandran, S.; Lee, C. D.; Ware, T. H. Tough, Shape-Changing Materials: Crystallized Liquid Crystal Elastomers. *Macromolecules* **2017**, *50*, 4267–4275.